Attempting to Verify the Existence of ZnY 2 O 4 Using Electron Backscatter Diffraction

Wolfgang Wisniewski, Peter Švančárek, Mathieu Allix

ACS OMEGA

http://pubs.acs.org/journal/acsodf

Article

Attempting to Verify the Existence of ZnY_2O_4 Using Electron Backscatter Diffraction

Wolfgang Wisniewski,* Peter Švančárek, and Mathieu Allix

Cite This: *ACS Omega* 2020, 5, 17576−17581

Read Online

ACCESS | Metrics & More | Article Recommendations

ABSTRACT: Attempts to synthesize ZnY_2O_4 are made via a solid-state reaction in a high-temperature X-ray powder diffraction chamber as well as analyzing Y_2O_3 sinter ceramics pressure infiltrated by ZnO in a scanning electron microscope using energy-dispersive X-ray spectroscopy and electron backscatter diffraction (EBSD). The microstructure of the sinter ceramic is composed of ZnO grains dispersed in an Y_2O_3 matrix. Superimposed EBSD patterns of Y_2O_3 are misindexed as ZnY_2O_4 during the EBSD scan. The literature concerning ZnY_2O_4 is critically discussed.

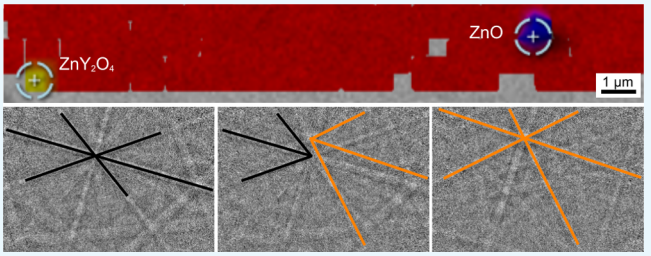

INTRODUCTION

Creating new phases with interesting properties is a general goal in materials science. Often these properties are significantly affected by the microstructure in which the phases occur, meaning that the production process leading to the phase plays a vital role for the resulting material. One topic in this field of research is combining ZnO and Y_2O_3 as well as various dopants, *e.g.*, in the search for better luminescence materials.[1−4] In this context, it has been proposed that Zn, Y, and O may form a compound of the composition ZnY_2O_4.

ZnY_2O_4 is a phase only mentioned in the literature three times to the best of our knowledge: first in 1979[5] and theoretically considered assuming a cubic spinel structure in 2015 when it was concluded that such a phase might be an interesting solar cell material.[6] In that same year, a material with the composition ZnY_2O_4 was reported to be synthesized from $Zn(NO_3)_2$ and $Y(NO_3)_3$ via a sol−gel process in the form of nanoparticles and analyzed with respect to its crystal structure and magnetic properties.[7] The JCPDS file no. 04-022-8399 for ZnY_2O_4 based on ref 7 was entered in 2018.

Figure 1 presents an XRPD pattern redrawn based on the experimental pattern presented in ref 7 in comparison to the plotted theoretical patterns of ZnY_2O_4, ZnO, and Y_2O_3. There are obvious discrepancies between the redrawn experimental pattern and the JCPSD file 04-022-8399, both with respect to the positions of the peaks as well as their intensity. Furthermore, all of the major peaks in the experimental pattern can be attributed to either ZnO or Y_2O_3, raising the question whether the material synthesized in ref 7 was truly a single-phase material.

The structure analysis in ref 7 was performed using X-ray powder diffraction (XRPD) in the Θ-2Θ-setup, which is a method well suited to analyze crystalline nanoparticles if applied correctly.[8] However, ref 7 fails to state a number of

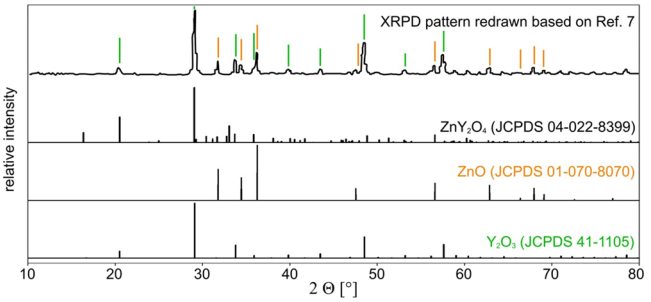

Figure 1. XRPD pattern redrawn based on Figure 1 in ref 7 in comparison to the JCPSD pattern no. 04-022-8399 and that of ZnO (01-070-8370) and Y_2O_3 (00-041-1105).

relevant details concerning the performed measurement: for example, the unit cell structure of the proposed ZnY_2O_4 is "developed on space group *Pccn*", *i.e.*, of orthorhombic symmetry, but there is no information why this space group is suited to describe the structure of the proposed phase or why it was chosen over the cubic structure assumed in ref 6. Furthermore, the authors state that the XRPD pattern results from a nanometer-size powder,[7] but the XRPD pattern does not show the peak broadening associated with such grain sizes.[8] The agreement factors values of *R* above 90% are highly questionable. There is no information regarding the structure determination process, and necessary details concerning the

Received: May 3, 2020
Accepted: June 26, 2020
Published: July 9, 2020

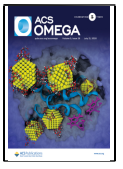

https://dx.doi.org/10.1021/acsomega.0c02043
ACS Omega 2020, 5, 17576−17581

performed Rietveld refinement are lacking, *e.g.*, the Rietveld fit is not presented.

Furthermore, the existence of the proposed ZnY_2O_4 was not verified by any second method: the authors state that, for an energy-dispersive X-ray spectroscopy (EDXS) analysis, "mapping of all the constituent elements individually shows uniform distribution of the elements indicating the homogeneity of the sample".[7] However, they also claim a grain size in the nanometer scale. As the information volume of EDXS usually exceeds an area of 1 μm in diameter (the applied acceleration voltage is not stated in ref 7, EDXS is not suited to resolve the composition of the proposed nanometer-sized grains. Microstructures containing multiple phases can appear homogeneous in an EDXS map[9,10] even if the crystals approach the micrometer scale in size; see, *e.g.*, the distribution of Mg in Figure 16d of ref 10.

An alternative method to discern phases in a scanning electron microscope (SEM) is electron backscatter diffraction (EBSD), which shows a much better spatial resolution,[11−14] although it should be noted that the full information volume of EBSD can exceed 100 nm in depth.[15,16] EBSD can be used to identify the phases of low content in crystalline microstructures, which fail to be detected by X-ray diffraction.[10,17−20] However, EBSD needs a homogeneous crystal lattice to function as a diffraction lattice and enable the formation of Kikuchi bands. Hence, EBSD is probably not suited to analyze the thin rods and small particles resulting from the previously proposed sol−gel process. Hence, reproducing the experimental approach of ref 7 is useless for a phase identification attempt based on EBSD.

An alternative approach to achieve the formation of ZnY_2O_4 via a chemical reaction is pressure infiltration where a water solution of zinc acetate is pressed into the pores of an Y_2O_3 ceramic and allowed to dry. Heating the resulting ZnO-filled Y_2O_3 ceramic to a temperature high enough to allow sintering should also allow a reaction between Y_2O_3 and the infiltrated ZnO. Hence, ZnY_2O_4 could form around pores and possibly along the grain boundaries adjacent to these pores in the host ceramic.

In this work, we investigate the solid-state interaction of Y_2O_3 and ZnO in a HT-XRPD chamber and analyze the microstructure of an Y_2O_3 ceramic pressure infiltrated with ZnO and sintered at 1500 °C using XRPD, SEM, EDXS, and EBSD in an attempt to locate a phase with the composition ZnY_2O_4.

RESULTS AND DISCUSSION

XRPD patterns acquired from the mixed powders of Y_2O_3 and ZnO at the respectively stated temperatures are presented in Figure 2. The patterns indicate no reaction between these powders, and ZnY_2O_4 is not indicated in any pattern. Even annealing these powders at 1200 °C for 5 h does not lead to any significant changes of the XRPD pattern with respect to ZnY_2O_4. While Zn has been added to Y_2O_3 ceramics[21−27] and, *e.g.*, shifts in XRD peaks indicate that Zn can enter the Y_2O_3 lattice, ZnY_2O_4 was never identified by XRPD after the performed experiments. A systematic analysis of the solubility of Zn in Y_2O_3 could not be found in the literature.

The pre-sintered Y_2O_3 ceramics showed relative densities of 40 ± 1%. They were subsequently infiltrated with the zinc acetate solution, dried, and sintered. Assuming a hypothetical phase of the composition $Zn_{0.07}Y_{1.93}O_{2.965}$ (with a calculated density of 5.024 g/cm^3 resulting from an assumed substitution

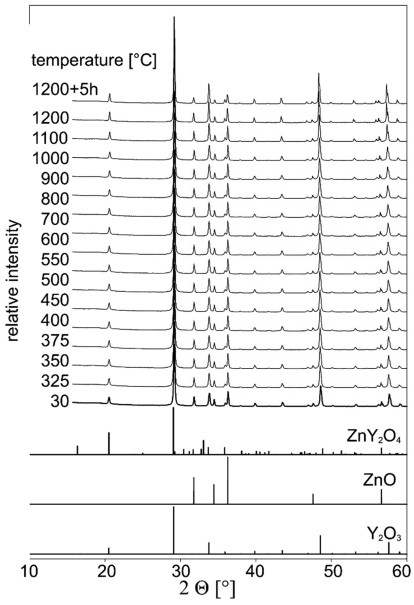

Figure 2. XRPD patterns acquired from the powder mixture of Y_2O_3 and ZnO at the stated temperatures. A final pattern obtained after annealing for 5 h at 1200 °C is also presented. The theoretical patterns of ZnY_2O_4 (JCPSD 04-022-8399), ZnO (JCPDS 01-070-8370), and Y_2O_3 (JCPDS 00-041-1105) are presented for comparison.

of 3.5 at. % Zn (*i.e.*, 7.25 mol % ZnO with a density of 5.61 g/cm^3 and 92.75 mol % Y_2O_3 (5.01 g/cm^3)) with no porosity as a reference, the relative density of these Zn-infiltrated specimens reached 98.7 ± 0.6% after sintering. Figure 3

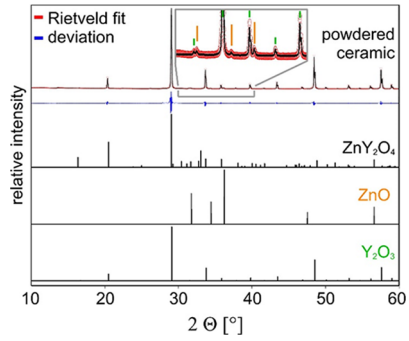

Figure 3. XRPD pattern acquired from a powder prepared from the sintered Y_2O_3 ceramic; the segment highlighted in gray is presented in greater detail, and the peaks are attributed to the respective phases. A Rietveld fit is presented (wR_p = 5.8%, R_p = 3.72%, GOF = 7.34) along with its deviation from the experimental pattern. The theoretical patterns of ZnY_2O_3 (JCPSD 04-022-8399), ZnO (JCPDS 01-070-8370), and Y_2O_3 (JCPDS 00-041-1105) are presented for comparison.

presents an XRPD pattern acquired from such a sintered sample along with a Rietveld fit regarding Y_2O_3 and ZnO as well as its deviation from the acquired pattern. The theoretical patterns of ZnY_2O_4, Y_2O_3, and ZnO are presented for comparison. The framed inset presents the highlighted region in greater detail so as to visualize the comparably weak peaks attributable to ZnO, which the analysis of the XRPD pattern indicated to amount to 2.0(1) wt % in the sample. Further unattributed peaks of minor intensity occur in the pattern, but ZnY_2O_4 is not reliably indicated as, *e.g.*, the third most intense

https://dx.doi.org/10.1021/acsomega.0c02043
ACS Omega 2020, 5, 17576−17581

peak at 2Θ = 16.358° does not occur. The two most intense peaks in the JCPDS file no. 04-022-8399 match intense peaks of Y_2O_3.

An SEM micrograph obtained from a cross section through the sintered ceramics infused with ZnO is presented in Figure 4a. EDXS maps illustrating the occurrence of Zn and Y are

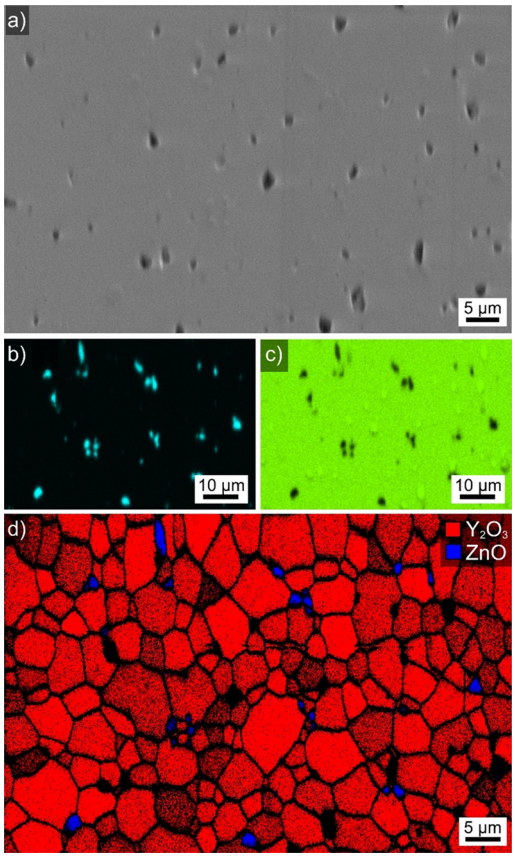

Figure 4. (a) SEM micrograph of the sintered ceramic. EDXS element maps of (b) Zn and (c) Y are presented along with (d) the phase map of an EBSD scan performed on the area.

presented in Figure 4b,c, respectively, while the phase map of an EBSD scan performed with only the material files of Y_2O_3 and ZnO is presented in Figure 4d. While the SEM micrograph indicated a porous microstructure, the EDXS maps indicated the presence of ZnO grains in an Y_2O_3 matrix. This impression is confirmed by the phase map as EBSD patterns were attributed to ZnO at most of the locations showing the elevated levels of Zn.

A few locations of elevated Zn content fail to provide EBSD patterns indexed as ZnO during the EBSD scan, but considering that the information depth of EDXS exceeds 1 μm when using the applied acceleration voltage of 15 kV while the information depth of EBSD is below 80 nm,[16] these locations probably mark ZnO grains located below the surface of the cross section. The ZnO grains confirm the successful infiltration of ZnO into the Y_2O_3 ceramic as already indicated by the XRPD results in Figure 3. However, the lack of a Zn signal along the Y_2O_3 grain boundaries indicates that ZnO probably did not significantly react with Y_2O_3 during sintering. As the ZnO grains probably formed in the pores of the pre-sintered ceramic during the infiltration process, some of the pores discernible in Figure 4a may result from ZnO particles being pulled from the ceramic during sample preparation.

Nevertheless, a material file built based on the crystallographic data in ref 7 was created and provided during further EBSD analysis in an attempt to locate the proposed ZnY_2O_4 phase. Figure 5 presents the phase map of an EBSD scan

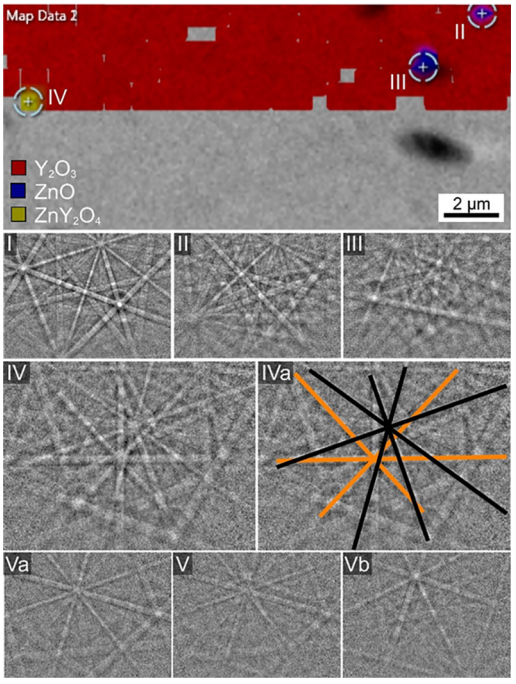

Figure 5. Phase map of an EBSD scan superimposed onto an SEM micrograph of the sample surface. EBSD pattern I represents the Y_2O_3 pattern quality obtained from this sample. The EBSD patterns II–IV were acquired at the locations II–IV in the phase map. Selected Kikuchi bands in pattern IV are highlighted in pattern IVa. Pattern V was acquired from the same surface, and the patterns Va and Vb were acquired immediately adjacent to pattern V.

superimposed onto and SEM-micrograph of the surface. While most of the data points are attributed to Y_2O_3, the locations II and III are attributed to ZnO and the location IV is attributed to ZnY_2O_4 by the indexing process. The presented EBSD pattern I is representative for the high-quality EBSD patterns obtained after the applied polishing procedure and indexed as Y_2O_3. The EBSD patterns II and III were acquired at the locations II and III and are indexed as ZnO. The EBSD pattern IV, however, contains components of two EBSD patterns, *i.e.*, it is the result of EBSD-pattern superposition. This problem is always a challenge for the indexing software as it can detect Kikuchi bands from both patterns. Selected Kikuchi bands are highlighted in pattern IVa to illustrate the problem: components from differing patterns are highlighted in orange or black. The pattern IV was acquired at the location IV and is indexed as ZnY_2O_4 by the software. EBSD pattern V was obtained from the same sample and is comparably indexed as ZnY_2O_4: it is also a superposition of the patterns Va and Vb (both indexed as Y_2O_3) acquired from adjacent locations.

As all individually acquired EBSD patterns indexed as ZnY_2O_4 showed clear signs of EBSD-pattern superposition, it is doubtful whether any of the data points attributed to ZnY_2O_4 in the EBSD scan of this sample actually originate from ZnY_2O_4.

https://dx.doi.org/10.1021/acsomega.0c02043
ACS Omega 2020, 5, 17576–17581

Comparably superimposed EBSD patterns were obtained from comparably prepared samples: while most of them fail to be indexed or are indexed as either Y_2O_3 or ZnO, a few are again indexed as ZnY_2O_4. In order to test the hypothesis that all data points attributed to ZnY_2O_4 by the indexing process (8 bands detected, Hough resolution 60, and 40 to 44 reflectors activated for each phase) suffer from pattern superposition, a set scan frame was started three times with increasing EBSD-pattern quality settings, *i.e.*, using a binning of 8 × 8, 4 × 4, and finally 2 × 2. The resulting phase maps are presented in Figure 6 along with the data point fraction attributed to the respective phases provided for indexing and the band contrast (BC) map of the scan performed using a binning of 2 × 2.

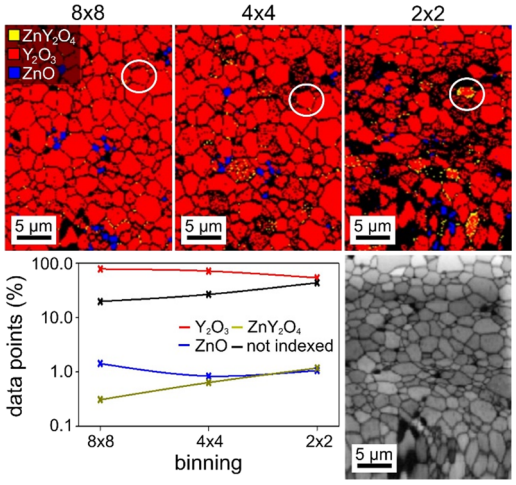

Figure 6. Phase maps of EBSD scans performed on the same area using constant settings but reducing the binning from 8 × 8 to 4 × 4 and finally 2 × 2. The resulting fractions of data points attributed to the respective phases are plotted. The BC map (grayscale) of the scan performed using a binning of 2 × 2 is also presented.

The white circles highlight a grain where the top left neighbor increasingly fails to be indexed, and lower binning settings lead to more data points attributed to ZnY_2O_4. It is also clear that some drift occurred at the end of the 2 × 2 scan and the scans did not start at identical locations although neither the frame nor the sample was repositioned. Overall, the fraction of unindexed data points and data points attributed to ZnY_2O_4 increases with the decreasing binning setting.

Superpositioned patterns are problematic for indexing because the software detects Kikuchi bands by their intensity, always assuming that they are from only one crystal lattice. It has been shown that the information depth significant to an EBSD pattern increases with lower binning settings.[16] However, it should be noted that high-quality EBSD patterns actually have smaller information depth significant to their evaluation than low-quality patterns acquired with the same settings because the Hough transform detects the sharpest lines in the acquired Kukuchi patterns.[16]

Nevertheless, the effect of the EBSD-pattern superposition itself is more significant when analyzing high-quality patterns: the information volume contributing to the EBSD pattern obtained near, *e.g.*, a grain boundary, is more likely to include information from a neighboring grain. As most of the superpositioned EBSD patterns failed to be indexed, this is in agreement with the increasing rate of unindexed data points presented in Figure 6. As only a fraction of the superpositioned patterns were found to be indexed as ZnY_2O_4, increasing the fraction of unindexed data points should also lead to an increasing amount of data points indexed as ZnY_2O_4, matching the result indicated in Figure 6. Although this does not prove that ZnY_2O_4 does not exist in the analyzed ceramic, this result matches the expectation as a higher pattern quality increases the probability that weaker components of a secondary crystal lattice are detected for evaluation.

The drift during the scan performed with the 2 × 2 binning of course limits the comparability of the data point fractions in the scans, and it may be caused by the sample heating up.[28] The BC map of this scan additionally shows a general drop in pattern quality during the scan. However, this drop does not match the conditions outlined for EBSD-pattern degradation during a scan.[28] Furthermore, comparing the grain structure with that in the 4 × 4 scan shows that the 2 × 2 scan started with a slight shift. Hence, the observed drop in pattern quality results from the previous 4 × 4 scan, *i.e.*, via carbon accumulation or radiation damage. While this drop applies to all subsequent grains, only selected grains fail to be indexed by the software. Hence, it is unlikely that the slightly lower band contrast caused by the previous scans significantly affects the indexing process, remembering that a 2 × 2 binned pattern generally contains more details than a 4 ×4 binned pattern.

In summary, XRPD did not show any indication of the proposed ZnY_2O_4 and EDXS showed no indication of, *e.g.*, Zn^{2+} diffusion along grain boundaries. As all EBSD patterns indexed as ZnY_2O_4 but subjected to a detailed analysis were found to be superpositioned EBSD patterns of Y_2O_3, we conclude that ZnY_2O_4 probably does not occur in the prepared ceramics. As the ZnY_2O_4 reported in ref 7 was produced via a sol−gel route, it is unknown whether this phase is perhaps metastable and perhaps destroyed by high temperatures. In any case, it failed to be detected after the experiments presented here.

CONCLUSIONS

Powders of Y_2O_3 and ZnO were mixed and heated to 1200 °C in an XRPD chamber, but ZnY_2O_4 failed to be observed. Y_2O_3 ceramics containing 2.0(1) wt % ZnO were prepared by pressure infiltration and subsequent sintering. The ceramics contain discreet ZnO grains distributed in a matrix of Y_2O_3, and an interaction between these components is not indicated by any measurement. ZnY_2O_4 was not detected, and the data presented in ref 7 is insufficient to prove its existence. EBSD-pattern superposition can lead to misindexed EBSD patterns when using the applied software package.

Materials and Methods. Commercial powders of Y_2O_3 (Alfa Aesar, 99.99%) and ZnO (Alfa Aesar, 99.99%) were mixed in the mol ratio of 1:1 without drying or further milling. They were heated in an HT-XRPD HTK12 Anton Paar chamber under a normal air atmosphere using a heating rate of 0.5°/s. *In situ* XRPD measurements were performed on a Bragg−Brentano D8 Advance Bruker laboratory diffractometer equipped with a Vantec-1 detector opened at 8° using Cu Kα radiation. XRPD patterns were acquired from 2θ = 12−90° with a 0.024° step size and a measuring time of 0.25 s/step from room temperature up to 1200 °C (the maximum temperature is safely achievable in the available chamber), and XRPD patterns were acquired every 25 °C. The measurements were started as soon as the respective temperature was reached, *i.e.*, an equilibrium time was not applied.

https://dx.doi.org/10.1021/acsomega.0c02043
ACS Omega 2020, 5, 17576−17581

Ceramic Y_2O_3 green bodies were prepared by pressure filtrating a suspension of isopropanol ($(CH_3)_2CHOH$, p.a., 99.7%+, CentralChem, Slovakia) containing 5 vol % Y_2O_3 powder (PENGDA, 150 nm grain size, no further milling, dried by storing over silica gel) and stabilized by 1 wt % polyethylene glycol (PEG, 400 Ultra-pure, Fluka, Germany), and the Y_2O_3 mass serving as the reference. The green bodies were dried in an oven at 40 °C for at least 12 h to evaporate the isopropanol. A superkanthal furnace (Classic, Czech republic) was used to pre-sinter the green bodies in an ambient atmosphere via a step of heating to 1000 °C with 10 °C/min. They were held for 1 h before turning the furnace off, allowing the samples to cool. The resulting pellets were porous but sufficiently stable and able to withstand the infiltration procedure. The density of pre-sintered samples was determined by measuring their mass (using a KERN 770-14 scale with a precision of ±1 mg) and dimensions (using a METROLA micrometer screw with a precision of ±10 μm).

A zinc acetate water solution ($Zn(CH_3COO)_2{\cdot}2H_2O$ p.a. CentralChem, Slovakia) was used to infiltrate the pre-sintered pellets with 3.5 at. % additive Zn. The infiltrated pellets were sintered in a superkanthal furnace (Classic, Czech republic) under an ambient atmosphere. The temperature regime included heating to 80 °C where the samples were held for 2 h before heating them to 250 °C where they were held for another 2 h and finally heated to 1500 °C where they sintered for another 2 h before the furnace was turned off, allowing the samples to cool. All heating rates were 10°/min. The density of the sintered specimens was determined using the Archimedes method with water as the immersion medium and by weighing the specimens in air as well as water using an OHAUS Explorer scale with a precision of ±1 mg.

XRPD of the sintered ceramics was performed with Cu Kα radiation in the $\theta-2\theta$ arrangement using a PANalytical Empyrean DY1098 X-ray powder diffractometer and a 0.013° step size.

Cross sections for analysis in the SEM were prepared and embedded in Buehler KonductoMet by pressure molding at 150 °C for 1 min. They were ground and polished using diamond with decreasing grain sizes from 45 to 0.5 μm in a Buehler AutoMet 300 polisher. A final finish of 2−6 h vibration polishing was applied using a Buehler VibroMet 2 with a static load of 200 g and a MasterPrep polishing suspension (50 nm sol−gel alumina). The polished cross sections were coated with a thin layer of a Au/Pd (80/20) alloy at approximately 5 Pa to avoid surface charging.

SEM analyses were performed using a Jeol JSM 7600F SEM equipped with an X-Max 50 mm^2 EDXS detector (Oxford Instruments) and a Nordlis Max EBSD camera. EDXS spot measurements were acquired using acceleration voltages of 15−20 kV. EBSD scans were performed using an acceleration voltage of 15 kV and a current of up to ca. 3 nA. The EDXS and EBSD scans were captured using the Oxford Instruments software Aztec 3.1 coupled with the Channel 5 software.

AUTHOR INFORMATION

Corresponding Author

Wolfgang Wisniewski − *CEMHTI UPR3079 CNRS, Univ. Orléans, Orléans F-45071, France; Le Studium, Loire Valley Institute for Advanced Studies, Orléans & Tours 45000, France;* orcid.org/0000-0001-6390-4750; Email: wolfgang.w@uni-jena.de

Authors

Peter Švančárek − *Joint Glass Centre of the IIC SAS, TnUAD, FChPT STU, Fun Glass, 911 50, Slovakia*

Mathieu Allix − *CEMHTI UPR3079 CNRS, Univ. Orléans, Orléans F-45071, France;* orcid.org/0000-0001-9317-1316

Complete contact information is available at: https://pubs.acs.org/10.1021/acsomega.0c02043

Notes

The authors declare no competing financial interest.

ACKNOWLEDGMENTS

Results incorporated in this paper have received funding from the European Union's Horizon 2020 research and innovation program under the Marie Skłodowska-Curie grant agreement no. 665790. This paper is also a part of dissemination activities of the project FunGlass. This project has received funding from the European Union's Horizon 2020 research and innovation program under grant agreement no 739566. This work was also supported by the Slovak Research and Development Agency under the contract no. APVV-17-0049 and by grant nos. VEGA 1/0527/18 and VEGA 2/0026/17.

REFERENCES

(1) Kumar, V.; Bishnoi, S.; Kotnala, R. K.; Chawla, S. Monochromatic orange emission under blue and Green excitation fromEu^{3+} doped ZnO-Y_2O_3 luminomagnetic microcomposite. *J. Lumin.* **2016**, *179*, 100−106.

(2) Su, T.-M.; Qin, Z.-Z.; Ji, H.-B.; Jiang, Y.-X. Preparation, Characterization, and Activity of Y_2O_3-ZnO Complex Oxides for the Photodegradation of 2,4-Dinitrophenol. *Int. J. Photoenergy* **2014**, *2014*, 794057.

(3) Ganjkhanlou, Y.; Hosseinnia, A.; Kazemzad, M.; Moghaddam, A. B.; Khanlarkhani, A. Y_2O_3: Eu, Zn nanocrystals as a fluorescent probe for the detection of biotin. *Microchim. Acta* **2012**, *177*, 473−478.

(4) Pandey, A.; Rai, V. K. Improved luminescence and temperature sensing performance of $Ho^{3+}-Yb^{3+}-Zn^{2+}$:Y_2O_3 phosphor. *Dalton Trans.* **2013**, *42*, 11005−11011.

(5) Dharmadhikari, D. M. Structural study of ZnY_2O_4. *Indian J. Phys.* **1979**, *4*, 459−460.

(6) Ghosh, A.; Kimari, A.; Rajagopalan, M.; Thangavel, R. Electronic structure of spinel oxides $ZnSc_2O_4$ and ZnY_2O_4: A first principle study. *AIP Conf. Proc.* **2015**, *1675*, No. 020010.

(7) Das, B. B.; Potu, V.; Ruppa, G. R. Synthesis, crystal structure and magnetic studies of ZnY_2O_4 oxide. *Indian J. Pure Appl. Phys.* **2015**, *53*, 399−403.

(8) Holder, C. F.; Schaak, R. E. Tutorial on Powder X-ray Diffraction for Characterizing Nanoscale Materials. *ACS Nano* **2019**, *13*, 7359−7365.

(9) Harizanova, R.; Wisniewski, W.; Avdeev, G.; Rüssel, C. Crystallization and growth morphology of barium titanate and fresnoite from a glass with the composition $20.1Na_2O{\cdot}23.1BaO{\cdot}23TiO_2{\cdot}9.8B_2O_3{\cdot}21SiO_2{\cdot}3Al_2O_3$. *CrystEngComm* **2017**, *19*, 6208−6214.

(10) Wisniewski, W.; Seidel, S.; Patzig, C.; Rüssel, C. Surface Crystallization of a MgO/ $Y_2O_3/SiO_2/Al_2O_3/ZrO_2$ Glass: Growth of an Oriented β-$Y_2Si_2O_7$ Layer and Epitaxial ZrO_2. *Sci. Rep.* **2017**, *7*, 44144.

(11) Zaefferer, S. On the formation mechanisms, spatial resolution and intensity of backscatter Kikuchi patterns. *Ultramicroscopy* **2007**, *107*, 254−266.

(12) Bhattacharyya, A.; Eades, J. A. Use of an energy filter to improve the spatial resolution of electron backscatter diffraction. *Scanning* **2009**, *31*, 114−121.

(13) Chen, D.; Kuo, J.-C.; Wu, W.-T. Effect of microscopic parameters on EBSD spatial resolution. *Ultramicroscopy* **2011**, *111*, 1488−1494.
(14) Chen, D.; Kuo, J.-C. The Effect of Atomic Mass on the Physical Spatial Resolution in EBSD. *Microsc. Microanal.* **2013**, *19*, 4−7.
(15) Wisniewski, W.; Rüssel, C. An Experimental Viewpoint on the Information Depth of EBSD. *Scanning* **2016**, *38*, 164−171.
(16) Wisniewski, W.; Saager, S.; Búbenroth, A.; Rüssel, C. Experimental Evidence Concerning the Significant Information Depth of Electron Backscatter Diffraction (EBSD). *Ultramicroscopy* **2017**, *173*, 1−9.
(17) Wisniewski, W.; Keshavarzi, A.; Zscheckel, T.; Rüssel, C. EBSD-based phase identification in glass-ceramics of the Y_2O_3-Al_2O_3-SiO_2 system containing α- and β-$Y_2Si_2O_7$. *J. Alloy. Compd.* **2017**, *699*, 832−840.
(18) Wisniewski, W.; Slavov, S.; Rüssel, C.; Dimitriev, Y. Phase Formation, Crystal Orientations and Epitaxy in Bi_2O_3/TiO_2/SiO_2(Nd_2O_3) Glass-Ceramics. *CrystEngComm* **2017**, *19*, 2775−2785.
(19) Wisniewski, W.; Slavov, S.; Rüssel, C.; Dimitriev, Y. Growing Oriented Layers of$Bi_4Ti_3O_{12}$in Bi_2O_3/TiO_2/SiO_2/Nd_2O_3/Al_2O_3Glass-Ceramics by Melt Quenching. *Sci. Rep.* **2018**, *8*, 8639.
(20) Wisniewski, W.; Fernandez-Carrion, A.; Schúppe, P.; Rüssel, C.; Allix, M. Oriented Nucleation and Crystal Growth in SrO-Al_2O_3-SiO_2 Tectosilicate Glasses. *CrystEngComm* **2018**, *20*, 3455−3466.
(21) Kominami, H.; Eguchi, C.; Kottaisamy, M.; Nakanishi, Y.; Hatanaka, Y. Synthesis of Zn-doped Y_2O_3 :Eu fine-particle phosphor by the sol-gel method. *J. Vac. Sci. Technol., B: Microelectron. Nanometer Struct.–Process., Meas., Phenom.* **2004**, *22*, 1386−1389.
(22) Jung, K. Y.; Han, K. H.; Ko, Y. S. Cathodoluminescence characteristics of particles and film of $(Y, Zn)_2O_3$:Eu phosphor prepared by spray pyrolysis. *J. Lumin.* **2007**, *127*, 391−396.
(23) Yadav, R.; Verma, S.; Rai, R. K. Intense white light emission in Tm^{3+}/Er^{3+}/Yb^{3+} co-doped Y_2O_3−ZnO nano-composit. *J. Phys. D: Appl. Phys.* **2013**, *46*, 275101.
(24) Lingadurai, K.; Sundarakannan, B.; Nagarajan, E. R.; Kominami, H.; Nakanishi, Y.; Kottaisamy, M. Low voltage cathode-luminescentproperties of Znco-doped Y_2O_3: Eu redphosphor. *J. Lumin.* **2016**, *177*, 249−253.
(25) Kumar, V.; Bullis, G.; Wang, G. Investigation of NIR-to-red upconversion luminescence mechanism inY_2O_3:Er^{3+},Yb^{3+} and the effect of co-doping Zn in the matrix. *J. Lumin.* **2017**, *192*, 982−989.
(26) Vasanthi, V.; Kottaisamy, M.; Ramakrishnan, V. Yellow and warm white light emitting Zn doped Y_2O_3 for near UV excitable phosphor converted WLED. *J. Mater. Sci.:Mater. Electron.* **2018**, *29*, 19724−19731.
(27) Kim, C.; Lee, D.; Lee, J.-A.; Lee, J.-H.; Heo, Y.-W.; Kim, J.-J. Effect of ZnO and TiO_2 doping on the sintering behavior of Y_2O_3 ceramics. *Ceram. Int.* **2019**, *45*, 13315−13318.
(28) Wisniewski, W.; Vúlksch, G.; Rüssel, C. The degradation of EBSD-patterns as a tool to investigate surface crystallized glasses and to identify glassy surface layers. *Ultramicroscopy* **2011**, *111*, 1712−1719.

https://dx.doi.org/10.1021/acsomega.0c02043
ACS Omega 2020, 5, 17576−17581